J|A|C|S ARTICLES

Published on Web 08/10/2010

Torsionally Responsive C_3-Symmetric Azo Dyes: Azo−Hydrazone Tautomerism, Conformational Switching, and Application for Chemical Sensing

Ho Yong Lee, Xinli Song, Hyunsoo Park, Mu-Hyun Baik, and Dongwhan Lee*

Department of Chemistry, Indiana University, 800 East Kirkwood Avenue, Bloomington, Indiana 47405

Received June 11, 2010; E-mail: dongwhan@indiana.edu

Abstract: An efficient triple azo coupling reaction between anilines and phloroglucinol furnished a series of C_3-symmetric molecules **7**−**9** supporting multiple conjugation pathways that converge at the molecular core. A combination of $^1H/^{13}C$ NMR spectroscopy, X-ray crystallography, and density functional theory computational studies provided a coherent picture of the [*n*,π]-conjugated molecular core, which is best described as the tris(hydrazone) [rather than tris(azo)] tautomer stabilized by resonance-assisted hydrogen bonding. For a homologous series of compounds, an increase in the torsional angles between the planar molecular core and the peripheral aryl groups results in a systematic blue shift in the low-energy electronic transitions (**7**, 523 nm; **8**, 505 nm; **9**, 445 nm in $CHCl_3$) that qualitatively correlates with the shrinkage of effective conjugation through structural distortion. Similar spectral shifts could also be induced by amine substrates that interact with the intramolecular hydrogen-bonding network to trigger bond-twisting motions. Specifically, a brief exposure of a thin film of **7** to vapor samples of butyl-, hexyl-, diethyl-, and diisopropylamine resulted in a rapid and reversible color change from pink to dark-orange. Under similar conditions, however, triethylamine did not elicit any detectable color change, despite the fact that it has a significantly higher vapor pressure than *n*-hexylamine. These findings implicate that the hydrogen-bonding donor ability is a key requirement for the binding-induced conformational switching, which allows for direct naked-eye detection of volatile amines under ambient conditions.

Introduction

Conjugation pathways supported by rigid π-skeletons can be modified by either covalent or noncovalent interactions, thereby offering opportunities to tune the optoelectronic properties inherent in extended electronic structures.[1−10] An increasing number of sensory systems have now been built on this principle, in which binding-induced conformational change along the π-backbone is tightly coupled to changes in the optical or electrochemical signal output.[2,10−12] Continuing challenges in such efforts lie in the invention and elaboration of new functional-group-rich π-conjugated platforms that can be (i)

(1) (a) Berresheim, A. J.; Müller, M.; Müllen, K. *Chem. Rev.* **1999**, *99*, 1747–1785. (b) Watson, M. D.; Fechtenkötter, A.; Müllen, K. *Chem. Rev.* **2001**, *101*, 1267–1300.

(2) (a) McQuade, D. T.; Pullen, A. E.; Swager, T. M. *Chem. Rev.* **2000**, *100*, 2537–2574. (b) Thomas, S. W., III; Joly, G. D.; Swager, T. M. *Chem. Rev.* **2007**, *107*, 1339–1386.

(3) Thematic issue on organic electronics and optoelectronics: *Chem. Rev.* **2007**, *107*, 923−1386.

(4) (a) Hoeben, F. J. M.; Jonkheijm, P.; Meijer, E. W.; Schenning, A. P. H. J. *Chem. Rev.* **2005**, *105*, 1491–1546. (b) De Greef, T. F. A.; Smulders, M. M. J.; Wolffs, M.; Schenning, A. P. H. J.; Sijbesma, R. P.; Meijer, E. W. *Chem. Rev.* **2009**, *109*, 5687–5754.

(5) *Functional Organic Materials*; Müller, T. J. J., Bunz, U. H. F., Eds.; Wiley-VCH: Weinheim, Germany, 2007.

(6) Elbing, M.; Bazan, G. C. *Angew. Chem., Int. Ed.* **2008**, *47*, 834–838.

(7) (a) Anthony, J. E. *Chem. Rev.* **2006**, *106*, 5028–5048. (b) Anthony, J. E. *Angew. Chem., Int. Ed.* **2008**, *47*, 452–483.

(8) For recent reviews on boron-containing π-conjugation and its modification by interaction with Lewis bases, see: (a) Yamaguchi, S.; Wakamiya, A. *Pure Appl. Chem.* **2006**, *78*, 1413–1424. (b) Jäckle, F. *Coord. Chem. Rev.* **2006**, *250*, 1107–1121. (c) Hudnall, T. W.; Chiu, C.-W.; Gabbai, F. P. *Acc. Chem. Res.* **2009**, *42*, 388–397. (d) Hudson, Z. M.; Wang, S. *Acc. Chem. Res.* **2009**, *42*, 1584–1596.

(9) For selected examples of covalent modification of rigid π-skeletons with main-group elements, see: (a) Yamaguchi, S.; Xu, C.; Okamoto, T. *Pure Appl. Chem.* **2006**, *78*, 721–730. (b) Fukazawa, A.; Yamada, H.; Yamaguchi, S. *Angew. Chem., Int. Ed.* **2008**, *47*, 5582–5585. (c) Wakamiya, A.; Mori, K.; Yamaguchi, S. *Angew. Chem., Int. Ed.* **2007**, *46*, 4273–4276. (d) Wakamiya, A.; Taniguchi, T.; Yamaguchi, S. *Angew. Chem., Int. Ed.* **2006**, *45*, 3170–3173. (e) Xu, C.; Wakamiya, A.; Yamaguchi, S. *J. Am. Chem. Soc.* **2005**, *127*, 1638–1639. (f) Takimiya, K.; Ebata, H.; Sakamoto, K.; Izawa, T.; Otsubo, T.; Kunugi, Y. *J. Am. Chem. Soc.* **2006**, *128*, 12604–12605. (g) Takimiya, K.; Kunugi, Y.; Konda, Y.; Ebata, H.; Toyoshima, Y.; Otsubo, T. *J. Am. Chem. Soc.* **2006**, *128*, 3044–3050. (h) Su, H.-C.; Fadhel, O.; Yang, C.-J.; Cho, T.-Y.; Fave, C.; Hissler, M.; Wu, C.-C.; Réau, R. *J. Am. Chem. Soc.* **2006**, *128*, 983–995. (i) Dienes, Y.; Durben, S.; Kárpáti, T.; Neumann, T.; Englert, U.; Nyulászi, L.; Baumgartner, T. *Chem.—Eur. J.* **2007**, *13*, 7487–7500. (j) Baumgartner, T.; Bergmans, W.; Kárpáti, T.; Neumann, T.; Nieger, M.; Nyulászi, L. *Chem.—Eur. J.* **2005**, *11*, 4687–4699.

(10) For binding-induced conformational switching of linearly π-conjugated molecules, see: (a) Inouye, M.; Waki, M.; Abe, H. *J. Am. Chem. Soc.* **2004**, *126*, 2022–2027. (b) Barboiu, M.; Lehn, J.-M. *Proc. Natl. Acad. Sci. U.S.A.* **2002**, *99*, 5201–5206. (c) Prince, R. B.; Okada, T.; Moore, J. S. *Angew. Chem., Int. Ed.* **1999**, *38*, 233–236. (d) Chang, K.-J.; Kang, B.-N.; Lee, M.-H.; Jeong, K.-S. *J. Am. Chem. Soc.* **2005**, *127*, 12214–12215. (e) Juwarker, H.; Lenhardt, J. M.; Pham, D. M.; Craig, S. L. *Angew. Chem., Int. Ed.* **2008**, *47*, 3740–3743. (f) Meudtner, R. M.; Hecht, S. *Angew. Chem., Int. Ed.* **2008**, *47*, 4926–4930.

(11) Riddle, J. A.; Jiang, X.; Lee, D. *Analyst* **2008**, *133*, 417–422.

(12) (a) McFarland, S. A.; Finney, N. S. *J. Am. Chem. Soc.* **2001**, *123*, 1260–1261. (b) McFarland, S. A.; Finney, N. S. *J. Am. Chem. Soc.* **2002**, *124*, 1178–1179.

Scheme 1. Conformational Switching between the Folded and Unfolded Conformations of Tris(*N*-salicylideneamine)

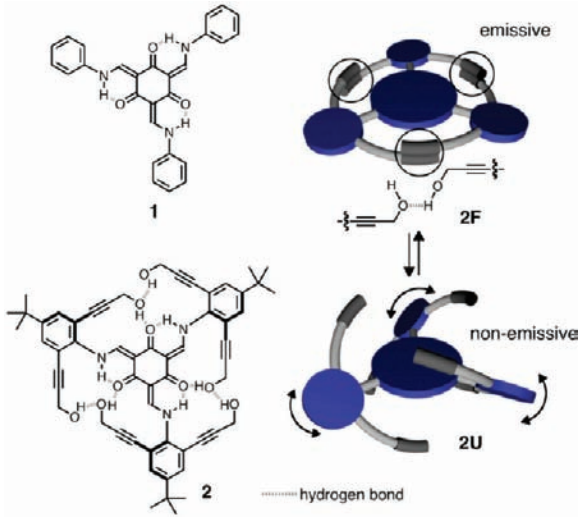

readily prepared from simple building blocks and (ii) easily modified via orthogonal synthetic operations on simple precursors.

We have previously reported a facile route for constructing tris(*N*-salicylideneamine)[13,14]-based conjugated chemical structures (Scheme 1).[15−22] The C_3-symmetric molecular core of the prototypical molecule **1** supports branched two-dimensional (2D) conjugation that radially extends to three aryl groups. In addition to modulation of the degree of conjugation between the $[n,\pi]$-conjugated core and the peripheral π extensions, torsional motions about the C−N bonds around the threefold-symmetric molecular core control the excitation and de-excitation pathways of these conformationally nonrigid fluorophores.[11]

Taking advantage of this structure−property relationship, we have shown that an intramolecular hydrogen-bonding network can be introduced to the peripheral aryl groups in **2** in order to drive the two-state switching between the "folded" conformer **2F** and the "unfolded" conformer **2U** (Scheme 1). External stimuli such as solvation, binding of an anion, or thermal energy thus elicit a reversible change in fluorescence and/or circular dichroism (for chiral derivatives).[18−22]

As shown in Scheme 2, the parent tris(*N*-salicylideneamine) system **1** can readily be constructed by a triple Schiff base

Scheme 2. Synthesis of C_3-Symmetric Chromophores **1** and **4** [as the $\mathbf{4}_H$ (=Hydrazone) or $\mathbf{4}_A$ (=Azo) Tautomer] by Triple Schiff Base Condensation (for **1**) and Triple Azo Coupling (for **4**)

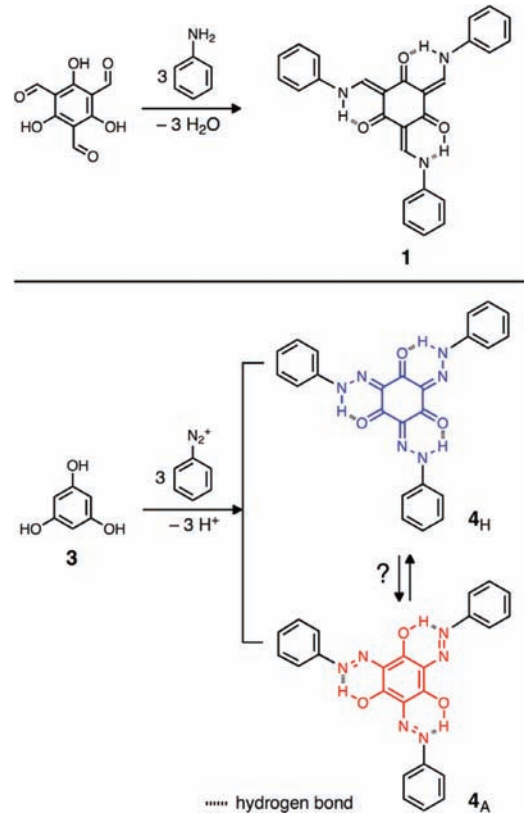

condensation reaction between 1,3,5-triformylphloroglucinol and primary amines. A close inspection of the keto−enamine molecular core of **1** logically suggests that a conceptually related C_3-symmetric platform **4** should readily be constructed by a triple azo coupling onto phloroglucinol (**3**) to formally replace the three CH−NH fragments in **1** with essentially isostructural N−NH units. In fact, the preparation of the parent "tris(phenylazo)phloroglucinol" **4** (Scheme 2; initially proposed as the azo tautomer $\mathbf{4}_A$) was described by Perkin as early as in 1897,[23] but only a handful of reports on its characterization have appeared since then.[24−29]

Intriguingly, the core tautomerism of **4** remains ambiguous even today, more than a century after its initial synthesis. The term "phenylazo", which has typically been used to describe **4**

(13) (a) Chong, J. H.; Sauer, M.; Patrick, B. O.; MacLachlan, M. J. *Org. Lett.* **2003**, *5*, 3823–3826. (b) Sauer, M.; Yeung, C.; Chong, J. H.; Patrick, B. O.; MacLachlan, M. J. *J. Org. Chem.* **2006**, *71*, 775–788.
(14) (a) Yelamaggad, C. V.; Achalkumar, A. S.; Rao, D. S. S.; Prasad, S. K. *J. Am. Chem. Soc.* **2004**, *126*, 6506–6507. (b) Yelamaggad, C. V.; Achalkumar, A. S.; Rao, D. S. S.; Prasad, S. K. *J. Org. Chem.* **2007**, *72*, 8308–8318. (c) Yelamaggad, C. V.; Achalkumar, A. S.; Rao, D. S. S.; Prasad, S. K. *J. Mater. Chem.* **2007**, *17*, 4521–4529. (d) Yelamaggad, C. V.; Achalkumar, A. S.; Rao, D. S. S.; Prasad, S. K. *J. Org. Chem.* **2009**, *74*, 3168–3171.
(15) Opsitnick, E.; Lee, D. *Chem.—Eur. J.* **2007**, *13*, 7040–7049.
(16) Riddle, J. A.; Bollinger, J. C.; Lee, D. *Angew. Chem., Int. Ed.* **2005**, *44*, 6689–6693.
(17) Riddle, J. A.; Lathrop, S. P.; Bollinger, J. C.; Lee, D. *J. Am. Chem. Soc.* **2006**, *128*, 10986–10987.
(18) Jiang, X.; Bollinger, J. C.; Lee, D. *J. Am. Chem. Soc.* **2006**, *128*, 11732–11733.
(19) Jiang, X.; Vieweger, M. C.; Bollinger, J. C.; Dragnea, B.; Lee, D. *Org. Lett.* **2007**, *9*, 3579–3582.
(20) Lim, Y.-K.; Jiang, X.; Bollinger, J. C.; Lee, D. *J. Mater. Chem.* **2007**, *17*, 1969–1980.
(21) Riddle, J. A.; Jiang, X.; Huffman, J.; Lee, D. *Angew. Chem., Int. Ed.* **2007**, *46*, 7019–7022.
(22) Jiang, X.; Lim, Y.-K.; Zhang, B. J.; Opsitnick, E. A.; Baik, M.-H.; Lee, D. *J. Am. Chem. Soc.* **2008**, *130*, 16812–16822.
(23) Perkin, A. G. *J. Chem. Soc., Trans.* **1897**, *71*, 1154–1156.
(24) Parini, V. P.; Gudvilovich, I. V.; Sorokin, A. V. *Izv. Akad. Nauk SSSR* **1966**, 572–575.
(25) Aseeva, R. M.; Gudvilovich, I. V.; Berlin, A. A. *Izv. Akad. Nauk SSSR* **1967**, 2635–2640.
(26) Van der Auweraer, M.; Catry, C.; Chi, L. F.; Karthaus, O.; Knoll, W.; Ringsdorf, H.; Sawodny, M.; Urban, C. *Thin Solid Films* **1992**, *210−211*, 39–41.
(27) Ghisletta, M.; Jalett, H.-P.; Gerfin, T.; Gramlich, V.; Hegetschweiler, K. *Helv. Chim. Acta* **1992**, *75*, 2233–2242.
(28) Abrahams, B. F.; Egan, S. J.; Robson, R. *J. Am. Chem. Soc.* **1999**, *121*, 3535–3536.
(29) A particular subclass of this structural motif having sugar-appended phenyl groups, known as Yariv reagents, have found practical applications in biochemical assays as multivalent dyes for staining or isolating proteoglycans. See: (a) Yariv, J.; Rapport, M. M.; Graf, L. *Biochem. J.* **1962**, *85*, 383–388. (b) Basile, D. V.; Ganjian, I. *J. Agric. Food Chem.* **2004**, *52*, 7453–7456, and references cited therein.

and its derivatives,[23,26,29,30] might adequately denote their chemical origin (from azo coupling) but incorrectly depicts the true chemical structure (see below). As shown in Scheme 2, the [*n*,π]-conjugated core of **4** can be described as either the tris(keto−hydrazone) (commonly denoted as "hydrazone"; $\mathbf{4_H}$) or tris(azo−enol) (commonly denoted as "azo"; $\mathbf{4_A}$) form. Studies in the 1960′s using UV−vis spectroscopy proposed an equilibrium between $\mathbf{4_H}$ and $\mathbf{4_A}$ that was based on qualitative comparison with other azo-based chromophores.[24] A similar interpretation was made on the basis of the IR data for **4**, which display what had been considered to be the signatures of N═N, C═N, and C═O bond-stretching frequencies.[25] This assignment, however, was later challenged by solution ^{1}H NMR studies on a derivative of **4**,[27] in which the presence of two sets of proton resonances was explained by invoking two slowly exchanging tris(hydrazone) isomers that have restricted rotation around the C−N bonds (see below). The only crystallographically characterized example of **4** is its deprotonated form $\mathbf{5}^{3-}$ (eq 1), which supports an $M_{12}L_8$-type cluster of copper(II).[28] As anticipated, the negative charge associated with the N,O-chelate is localized on the more electronegative oxygen atom, shifting the equilibrium toward the azo−enolate tautomer ($\mathbf{5_A}^{3-}$) rather than the keto−hydrazonate tautomer ($\mathbf{5_H}^{3-}$) (eq 1). Whether the same trend prevails for the neutral $\mathbf{4_H}$ versus $\mathbf{4_A}$ (Scheme 2) is an intriguing question, for which no structural evidence has been reported to date.

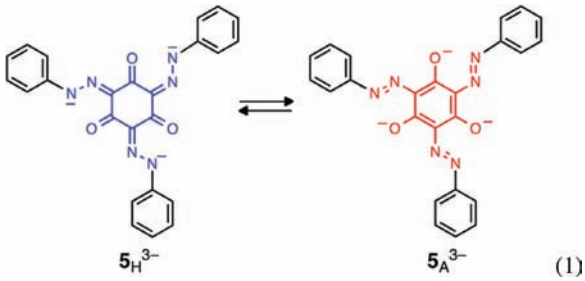

(1)

Azo dyes represent the most abundant class among commercial organic colorants, accounting for nearly 60% of the dyes currently available. In particular, the azo and hydrazone tautomers of hydroxyl azo compounds have been extensively studied, as the tautomeric state of such [*n*,π]-conjugated materials is directly related to the color profile.[31−33] Their rich photochemistry and the feasibility of modulating their optical properties through conformational switching have provided further impetus for our investigation of the previously underutilized azo-based chromophore **4**. Through a combination of experimental and theoretical studies, we have found that (i) the hydrogen-bonded molecular core of the formally "tris(azo)" phloroglucinol is best described as the keto−hydrazone rather than the enol−azo tautomer; (ii) the periphery of this robust C_3-symmetric [*n*,π] conjugation can be functionalized with bulky aryls to profoundly impact the conjugation pathways; and (iii) such torsion-dependent shifts in electronic transitions can further be exploited for the colorimetric sensing of amine vapors. The details of our findings are described in the following sections.

Scheme 3. Synthetic Routes to **7**−**9**[a]

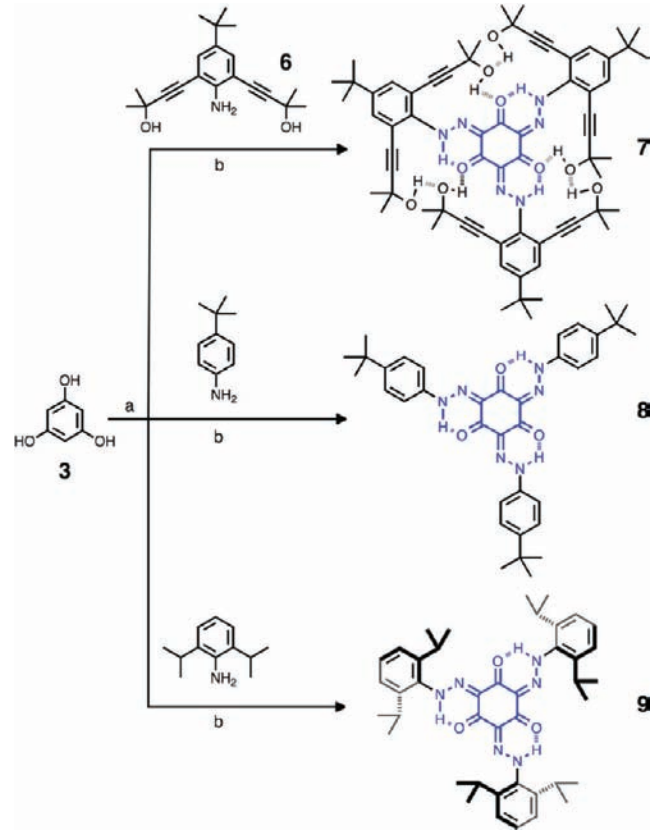

[a] Reaction conditions: (a) NaOH (2 M) in H_2O/MeOH, 0 °C. (b) (i) HCl (2 M) in H_2O/MeOH, 0 °C; (ii) $NaNO_2$, H_2O, 0 °C.

Results and Discussion

Synthesis and Tautomerism in Solution. As shown in Scheme 3, efficient triple azo coupling reactions between **3** and aniline derivatives furnished compounds **7**−**9** as bright-red solids (**7**, 81%; **8**, 34%; **9**, 82%) after purification by column chromatography. The ^{1}H NMR spectra of **7**−**9** in $CDCl_3$ (T = 298 K) display simple spectral patterns indicative of high molecular symmetry (Figure S1 in the Supporting Information). Notably, the significantly downfield-shifted resonances at >16 ppm suggest the presence of protons that engage in strong hydrogen bonding (Figure 1). This information alone, however, could not be used to distinguish between the azo and hydrazone tautomers (Scheme 2), as both have D−H···A (D = hydrogen-bond donor; A = hydrogen-bond acceptor) arrays disposed with threefold symmetry at the molecular core.

An initial clue for assigning the tautomeric state was provided by the ^{1}H NMR spectra obtained in DMSO-d_6. As shown in Figure 1d, **7** in DMSO-d_6 revealed the presence of two sets of downfield-shifted signals that reflect the presence of C_{3h} and C_s isomers in a ratio of ∼5:1 (Scheme 4). While the low energy barrier for rotation around the C−N single bonds in the azo tautomer would give rise to a single set of resonances as a population-averaged signal, the restricted rotation around the C═N double bonds in the hydrazone form would lead to two distinctive geometric isomers, one with local C_{3h} symmetry and

(30) (a) Pauling, L.; Pressman, D.; Campbell, D. H.; Ikeda, C.; Ikawa, M. *J. Am. Chem. Soc.* **1942**, *64*, 2994–3003. (b) Pressman, D.; Swingle, S. M.; Grossberg, A. L.; Pauling, L. *J. Am. Chem. Soc.* **1944**, *66*, 1731–1738.
(31) Christie, R. M. *Colour Chemistry*; Royal Society of Chemistry: Cambridge, U.K., 2001.
(32) Zollinger, H. *Color Chemistry: Syntheses, Properties, and Applications of Organic Dyes and Pigments*, 3rd ed.; VHCA: Zürich, Switzerland, 2003.
(33) Herbst, W.; Hunger, K. *Industrial Organic Pigments: Production, Properties, Applications*, 3rd ed.; Wiley-VCH: Weinheim, Germany, 2004.

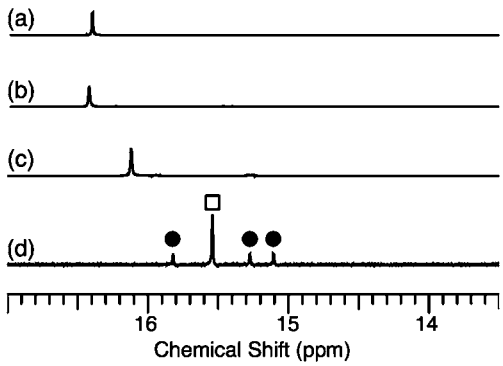

Figure 1. Partial ^{1}H NMR spectra of (a) **7**, (b) **8**, and (c) **9** in $CDCl_3$ at T = 298 K. The corresponding spectrum of **7** in DMSO-d_6 is shown in (d), in which peaks are assigned to two isomers of local C_{3h} (□) and C_s (●) symmetry (see Scheme 4).

Scheme 4. Azo versus Hydrazone Tautomerism and Geometric Isomerism of the Hydrazone Tautomer

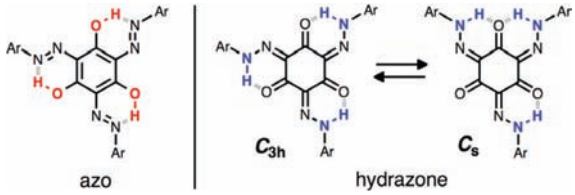

the other with C_s symmetry, as shown in Scheme 4.[27] A total of four unique N−H resonances were thus anticipated for the slowly exchanging isomers and were indeed observed experimentally (Figure 1d).

This interpretation is further supported by similar observations made for related tris(*N*-salicylideneamine) derivatives, in which the coexistence of two slowly interconverting isomers having C_{3h} and C_s symmetry with two independent sets of C_{vinyl}−H and $N_{enamine}$−H resonances is consistent with the keto−enamine rather than the enol−imine description of the core.[13,14,17]

A large number of azo dyes have a hydroxyl group at the ortho position, which not only prevents trans-to-cis isomerization[34,35] but also stabilizes the hydrazone form through resonance-assisted hydrogen bonding (RAHB).[36−41] For such constructs, the ^{13}C chemical shift has widely been used to assign the tautomeric state, since the phenolic and carbonyl carbon atoms have distinctively different resonances.[42−44] The ^{13}C NMR spectra of **7**−**9** obtained in $CDCl_3$ at T = 298 K (Figure 2)

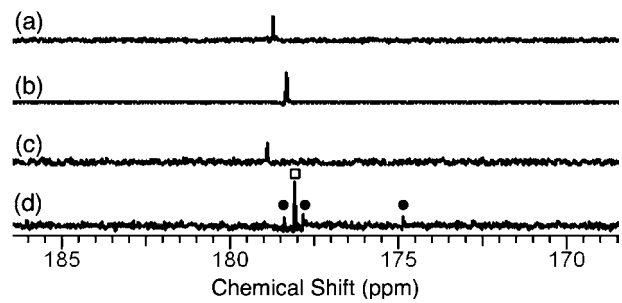

Figure 2. Partial ^{13}C NMR spectra of (a) **7**, (b) **8**, and (c) **9** in $CDCl_3$ at T = 298 K. The corresponding spectrum of **7** in DMSO-d_6 is shown in (d), in which peaks are assigned to two isomers of local C_{3h} (□) and C_s (●) symmetry (see Scheme 4).

supported the dominance of the hydrazone tautomer with the characteristic carbonyl carbon resonance at 178 ppm.[44] This parameter is close to the value of 174 ppm obtained by time-dependent density functional theory (TD-DFT) studies of the model compound $\mathbf{7'_H}$ (Scheme 5; see below). In DMSO-d_6, a total of four carbonyl resonances at 175−178 ppm were observed for **7** (Figure 2d), again confirming the presence of two slowly exchanging isomeric forms of the tris(hydrazone) tautomer (Scheme 4). Apparently, the hydrogen-bonding solvent DMSO raises the kinetic barrier for their structural interconversion on the NMR time scale. Over the temperature range from −40 to 50 °C, the N−H resonance of **7** at 16.4 ppm (in $CDCl_3$) remains essentially unchanged (Figure S2 in the Supporting Information). The characteristic carbon resonance at 178 ppm is also invariant under similar conditions (Figure S3 in the Supporting Information). These findings indicate that **7** mainly exists as the hydrazone form rather than as an equilibrium mixture of several tautomeric species.

Core Tautomerism: Computational Studies. The experimentally determined preference for the tris(hydrazone) rather than the tris(azo) tautomers of **7**−**9** in solution prompted theoretical investigations using DFT calculations. As highlighted in Scheme 2, the valence-bond description of the core tautomerism suggests that a cyclic array of keto−hydrazone fragments should formally destroy the aromaticity of the benzene ring at the core and thus be energetically disfavorable. We wished to gain a quantitative understanding of this seemingly counterintuitive bond rearrangement pattern resulting from triple azo coupling. DFT calculations on **7** and **8** were carried out using the simplified model compounds **7′** (Scheme 5) and **4** (Scheme 2), in which the *tert*-butyl groups on the aniline rings and the *gem*-dimethyl groups on the wing-tip tertiary alcohol fragments were replaced by hydrogen atoms to render the calculations computationally tractable. We expect these slight simplifications to have only a minor impact on the relative energetics of the two tautomers.

As summarized in Table 1, the difference between the solution-phase free energies of the two tautomeric forms was consistently large enough in favor of the tris(hydrazone) over the tris(azo) tautomer to justify the dominating presence of the former in an equilibrium situation. This general trend is maintained regardless of the structure of the aryl groups attached to the C_3-symmetric $\{C_6O_3(N_2H)_3\}$ core. The hydrazone tautomer $\mathbf{7'_H}$ is 15.93 kcal mol^{-1} lower in free energy than the azo tautomer $\mathbf{7'_A}$ in $CHCl_3$. For **4** and **9**, $\mathbf{4_H}$ and $\mathbf{9_H}$ are preferred over $\mathbf{4_A}$ and $\mathbf{9_A}$ by 17.43 and 11.87 kcal mol^{-1}, respectively. In more closely examining the structures of the two tautomers, subtle structural differences with potentially significant energetic consequences can be recognized.

(34) Natansohn, A.; Rochon, P. *Chem. Rev.* **2002**, *102*, 4139–4175.
(35) Kumar, G. S.; Neckers, D. C. *Chem. Rev.* **1989**, *89*, 1915–1925.
(36) Jeffrey, G. A. *An Introduction to Hydrogen Bonding*; Oxford University Press: New York, 1997.
(37) Gilli, P.; Bertolasi, V.; Pretto, L.; Lycka, A.; Gilli, G. *J. Am. Chem. Soc.* **2002**, *124*, 13554–13567.
(38) Gilli, P.; Bertolasi, V.; Pretto, L.; Antonov, L.; Gilli, G. *J. Am. Chem. Soc.* **2005**, *127*, 4943–4953.
(39) Gilli, P.; Pretto, L.; Bertolasi, V.; Gilli, G. *Acc. Chem. Res.* **2009**, *42*, 33–44.
(40) Gilli, G.; Gilli, P. *The Nature of the Hydrogen Bond*; Oxford University Press: New York, 2009.
(41) Sobczyk, L.; Grabowski, S. J.; Krygowski, T. M. *Chem. Rev.* **2005**, *105*, 3513–3560.
(42) Olivieri, A. C.; Wilson, R. B.; Paul, I. C.; Curtin, D. Y. *J. Am. Chem. Soc.* **1989**, *111*, 5525–5532.
(43) Alarcón, S. H.; Olivieri, A. C.; Sanz, D.; Claramunt, R. M.; Elguero, J. *J. Mol. Struct.* **2004**, *705*, 1–9.
(44) Shulishov, E. V.; Klimenko, I. P.; Korolev, V. A.; Kostyuchenko, I. V.; Okonnishnikova, G. P.; Tomilov, Y. V. *Russ. Chem. Bull., Int. Ed.* **2008**, *57*, 1703–1711.

Scheme 5. Chemical Structures of the DFT Models as Hydrazone (H) or Azo (A) Tautomers

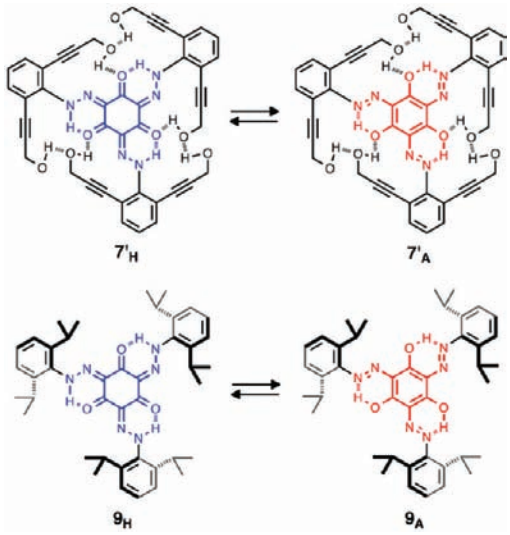

Table 1. Relative Energies (in kcal mol^{-1}) of the Tris(Hydrazone) Tautomers Referenced to the Corresponding Tris(Azo) Tautomers[a]

		ΔG	
	ΔH_{gas} (= ΔE + ZPE)	gas phase	in $CHCl_3$
7′	17.09	15.43	15.93
4	10.73	13.14	17.43
9	11.93	9.86	11.87

[a] $\Delta H_{gas} = H_{tris(azo)} - H_{tris(hydrazone)}$ and $\Delta G = G_{tris(azo)} - G_{tris(hydrazone)}$.

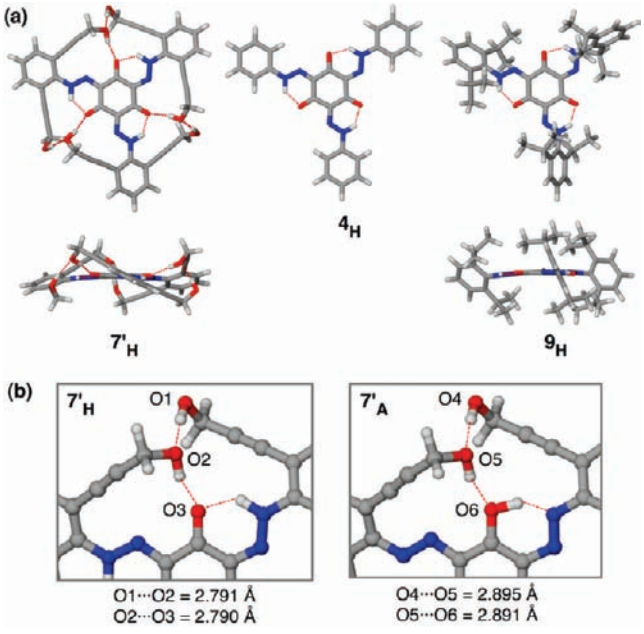

Figure 3. (a) Capped-stick representation of the DFT (B3LYP/6-31G**)-optimized geometries of models **7′$_H$**, **4$_H$**, and **9$_H$**. (b) Close-up view showing hydrogen bonds (dotted red lines) in **7′$_H$** (left) and **7′$_A$** (right) and O···O interatomic distances (see Table 2 for a list of relevant geometric parameters).

First, **4** maintains planar symmetry in both tautomers, whereas the steric demands of the peripheral decoration force the other two systems to deviate significantly from an overall planar geometry (Figure 3). The phenyl rings in **4** can therefore maintain a relatively strong π conjugation in both tautomers, with the interaction strength being greater in the resonance-stabilized **4$_A$** tautomer. As a consequence, the vibrational modes involving out-of-plane distortions of the peripheral moiety are shifted to higher energies in **4$_A$** relative to **4$_H$**, which in turn gives rise to a notable vibrational entropy penalty (see the Supporting Information) of nearly 2.5 kcal mol^{-1} at room temperature in the gas phase, increasing the energetic preference to 13.14 kcal mol^{-1}. In **7′** and **9**, however, the nonplanar arrangement weakens the π resonance between the peripheral and core moieties, so the entropic gain of having weaker C−O bonds dominates, affording an entropic preference for **7′$_A$** and **9$_A$** over their enthalpically preferred tautomers. The energetic preference for the tris(hydrazone) form is thus lessened to 15.43 and 9.86 kcal mol^{-1}, respectively, on the gas-phase free-energy surface. Whereas these are small effects, the sign of the correction amplifies the overall energetic impact, as demonstrated in the enthalpic and free-energy differences for the two tautomers **7′** and **4**. In the former, the enthalpic energy difference of 17.09 kcal mol^{-1} becomes 15.43 kcal mol^{-1} in gas-phase free energy, whereas in the latter case, the energy difference increases from 10.73 to 13.14 kcal mol^{-1}. Since the entropic differences are sensitive to the temperature, these intuitively understandable energy trends provide a rational design element that we intend to exploit further in future work. The impact of solvation is easy to understand by recognizing that in **4** the hydrazone/azo moieties are exposed to solvents, while they are shielded from solvent access to a certain degree in **7′** and **9**. Consequently, a greater differential solvation energy is computed for **4** than for the functionalized analogues.

Lastly, our DFT model demonstrates that **7′$_H$** has an additional array of hydrogen bonds connecting the OH groups on the ethynyl-extended wing tips of the peripheral aryl groups.[45] In addition to enhancing the conformational rigidity, the $O_{hydroxyl}$−H···$O_{hydroxyl}$−H···O_{ketone} cascade in **7′$_H$** (Figure 3b) should further stabilize the molecule relative to the alternative tautomer **7′$_A$** having the $O_{hydroxyl}$−H···$O_{hydroxyl}$−H···$O_{hydroxyl}$−H network (Figure 3b). In support of this notion, the O···O distance between the wing-tip OH group and the hydrogen-bonded oxygen atom at the molecular core is significantly shorter in **7′$_H$** (2.790 Å) than in **7′$_A$** (2.891 Å) (Figure 3b). As anticipated, the ketone oxygen atom in **7′$_H$** functions as a better hydrogen-bonding acceptor than the hydroxyl oxygen atom in **7′$_A$** and thus engages in a stronger hydrogen bond with the O−H group. These findings imply that secondary interactions with remotely located functional groups could further influence the energetics of tautomerization occurring at the molecular core. This intuitive interpretation is supported by the significantly larger energy difference (ΔH_{gas}) between **7′$_H$** and **7′$_A$** relative to those for the **4$_H$**−**4$_A$** and **9$_H$**−**9$_A$** pairs, which lack such interactions (Table 1).

Core Tautomerism: X-ray Crystallography. Direct experimental evidence to validate the DFT studies was obtained by single-crystal X-ray diffraction on **7** at T = 120 K. As shown in Figure 4, the planar {$C_6O_3(N_2H)_3$} core of **7**, with a mean deviation of 0.0128 Å from the least-squares plane, is supported by a cyclic bonding network that is arranged in a pseudo-C_3-symmetric fashion. The short interatomic distances between N and O [N(2)···O(2), 2.580(2) Å; N(4)···O(3), 2.519(3); N(6)···O(1), 2.592(2) Å] indicate that they are involved in strong hydrogen bonds assisted by resonance[36−41] in a manner similar to the situation in structurally characterized tris(*N*-salicylideneamine)s (Schemes 1 and 2).[13,16,18,20]

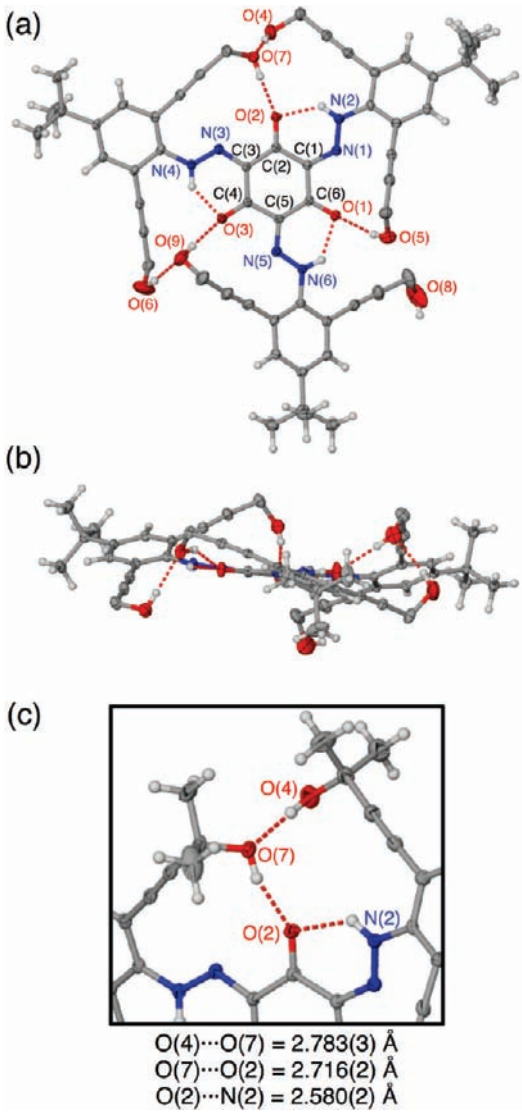

Figure 4. X-ray structure of **7** as ORTEP diagrams with thermal ellipsoids at 50% probability in which the *gem*-dimethyl groups have been omitted for clarity: (a) top view; (b) side view. (c) Close-up view showing hydrogen bonds (dotted red lines) and selected interatomic distances (see Table 3 for a full list).

A careful analysis of the crystallographically determined N−N, C−N, and C−O bond distances defining the six-membered "chelate" structure revealed that the bond metrics are comparable to those of the DFT model $\mathbf{7'_H}$ rather than the alternative tautomer $\mathbf{7'_A}$ (Table 2). In particular, the C═O double-bond character of the molecular core of **7** is evident in the bond distances of 1.244(3)−1.248(3) Å, which are close to the calculated parameter of 1.254 Å for the tris(hydrazone) DFT model $\mathbf{7'_H}$. In $\mathbf{7'_A}$, the corresponding C−O distance is significantly elongated to 1.322 Å, which clearly reflects the azo−enol character (Scheme 5 and Figure 3). In support of this notion, the difference electron density map of **7** (Figure 5) revealed

Table 2. Selected Bond Distances (in Å) from the X-ray Structure of **7** and the Corresponding Parameters in the DFT Models $\mathbf{7'_H}$ and $\mathbf{7'_A}$

	7	$\mathbf{7'_H}$	$\mathbf{7'_A}$
N(1)−N(2)	1.298(3)		
N(3)−N(4)	1.295(2)	1.295[a]	1.275[a]
N(5)−N(6)	1.295(3)		
O(1)−C(6)	1.248(3)		
O(2)−C(2)	1.244(3)	1.254[a]	1.322[a]
O(3)−C(4)	1.245(3)		
N(1)−C(1)	1.326(3)		
N(3)−C(3)	1.341(3)	1.337[a]	1.386[a]
N(5)−C(5)	1.332(3)		

[a] Calculated for the C_3-symmetric geometry.

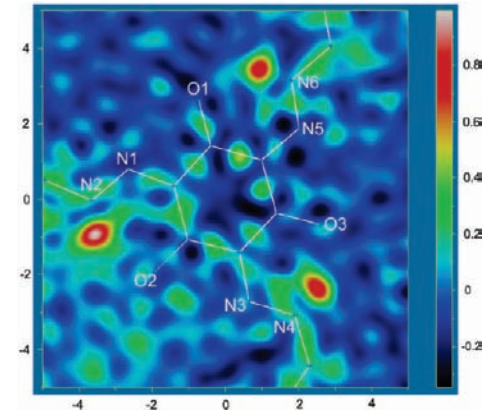

Figure 5. Difference Fourier map at 120(2) K computed in the mean plane of the $\{C_6O_3(N_2H)_3\}$ core of **7** after refinement was carried out with the hydrogen atoms excluded.[46]

Scheme 6. Azo ($\mathbf{10_A}$) versus Hydrazone ($\mathbf{10_H}$) Tautomer Equilibrium of 1-Phenylazo-2-hydroxynaphthol **10**

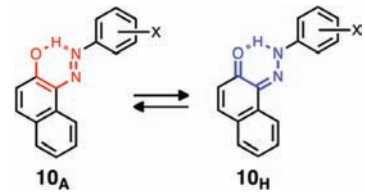

that the H atoms are located near the N atom rather than the O atom, which again is consistent with the hydrazone tautomer description.

As is evident from Table 2, the N−N, C−O, and C−N bond lengths are sensitive to the tautomeric state. In order to evaluate our own experimental findings against a larger set of structurally characterized azo vs hydrazone tautomers, we conducted a Cambridge Structural Database (CSD)[47] search on 1-phenylazo-2-hydroxynaphthol derivatives **10** (Scheme 6). This azo-based chromophore has been studied extensively because it is the basic structural unit of Sudan dyes, which are popular commercial organic colorants.[42,48−52] In addition, comprehensive studies of **10** using a combination of experimental and theoretical tools have significantly aided our understanding of RAHB.[37,38,53]

On the basis of a total of 49 reported structures,[54] plots of C−O versus C−N bond distances (Figure 6a) and C−O versus N−N bond distances (Figure 6b) were constructed for the systems that were assigned as the hydrazone tautomer $\mathbf{10_H}$ or a

(45) In a manner similar to the σ-bond cooperativity that is typically observed in extended networks of alcohols and phenols, this arrangement should polarize the participating O−H bonds and further strengthen the hydrogen bond.

(46) WinGX, version 1.70.01: Farrugia, L. J. *J. Appl. Crystallogr.* **1999**, *32*, 837–838.

(47) CSD, version 5.31 (last updates Feb 2010).

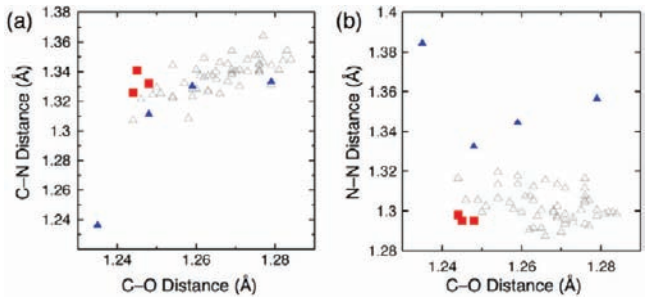

Figure 6. Plots of (a) C−O vs C−N and (b) C−O vs N−N bond distances. Data obtained from the CSD search are represented as triangles; blue triangles represent data for compounds **10a**−**d** (see Figure 7). Red squares represent data from the X-ray structure of **7**.

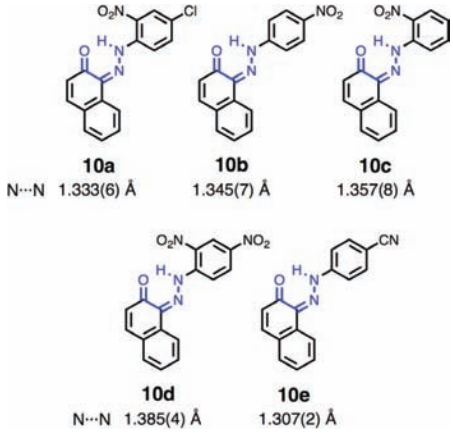

Figure 7. Chemical structures and crystallographically determined N−N bond distances of selected 1-phenylazo-2-hydroxynaphthols as the hydrazone tautomers.

fast-exchanging mixture with the azo tautomer $\mathbf{10_A}$ having a preference for $\mathbf{10_H}$. Similar empirical correlations were previously made for a larger set of data obtained from azo−hydrazone tautomers.[55] In our analysis, average bond distances of 1.305, 1.264, and 1.335 Å were determined for the N−N, C−O, and C−N bonds. The metric parameters determined experimentally for **7** and its DFT model $\mathbf{7'_H}$ (Table 2) are comparable to these values and fit within the range anticipated for the hydrazone structure (Figure 6).

During our comparative structural analysis, we noted that a series of 1-arylazo-2-hydroxynaphthols containing nitro groups (**10a**−**d**; Figure 7) have unusually long N−N bond distances of 1.333(6)−1.385(4) Å, while their C−O and C−N bond distances are comparable to those of others, except in the case of **10d** (Figure 6b).[56−59] Such elongated N−N bonds have occasionally been described as evidence for the hydrazone tautomer.[42,57,60,61] According to previous reports,[43,62,63] both **10b** and **10e** exist mainly as the hydrazone tautomers in solution, but the N−N bond distance in **10b** [1.345(7) Å] is significantly longer than that [1.307(2) Å][64] in **10e**. Increasing the number of nitro substituents, as in **10d**, results in a further lengthening of N−N bond to 1.385(4) Å. We suspect that not only the tautomeric state but also the electron-withdrawing effects of the nitro group might contribute to the lengthening of the N−N bond in **10a**−**d**. The use of the N−N bond distance as a sole criterion for assigning the azo−hydrazone tautomer state should thus be exercised with caution.

Table 3. Crystallographically Determined Interatomic Distances of Hydrogen Bonds Involving O−H Groups in **7**[a]

D−H···A	D···A distance (Å)	D−H···A angle (deg)
O(4)−H(4A)···O(7)	2.783(3)	178.3
O(5)−H(5A)···O(1)	2.998(3)	166.9
O(9)−H(9A)···O(3)	2.896(3)	176.8
O(7)−H(7A)···O(2)	2.716(2)	148.4
O(6)−H(6A)···O(9)	2.851(4)	170.4

[a] D = hydrogen-bond donor; A = hydrogen-bond acceptor.

Conformational Switching Assisted by Hydrogen Bonds. X-ray crystallographic studies of **7** also revealed that its wing-tip alcohol groups participate in an extensive intramolecular hydrogen-bonding network, such as O(4)−H(4)···O(7)−H(7)···O(2), which converges at the tris(hydrazone) molecular core (Figure 4). The O···O interatomic distances of the groups involved in such hydrogen bonds are listed in Table 3.

Notably, such pairwise contacts between terminal O−H groups bring the ethynyl-extended wing-tips into close proximity, thereby flattening the entire molecule, which has an average dihedral angle of $\tau = 23°$ between the molecular core and the peripheral aryl rings. The functional role of such $O_{hydroxyl}$−H···$O_{hydroxyl}$−H···O_{ketone} cascades was previously established for structurally analogous tris(*N*-salicylideneamine)s,[15,18−22] in which structural interconversion between the folded and unfolded conformations (Scheme 1) could be driven by the assembly and disassembly of such noncovalent contacts. A drastic change in the number of *torsional bonds* between the two conformers profoundly impacts the emission properties through opening and closing of nonradiative decay channels.[65]

In the solid state, however, one of the wing-tip OH groups in **7** is twisted away from the molecular core to engage in a weak *intermolecular* O−H···O hydrogen bond (O···O, 3.134

(48) Burawoy, A.; Salem, A. G.; Thompson, A. R. *J. Chem. Soc.* **1952**, 4793–4798.
(49) Simov, D.; Stojanov, S. *J. Mol. Struct.* **1973**, *19*, 255–274.
(50) Ball, P.; Nichols, C. H. *Dyes Pigm.* **1982**, *3*, 5–26.
(51) Antonov, L.; Stoyanov, S.; Stoyanova, T. *Dyes Pigm.* **1995**, *27*, 133–142.
(52) Özen, A. S.; Doruker, P.; Aviyente, V. *J. Phys. Chem. A* **2007**, *111*, 13506–13514.
(53) Gilli, P.; Bertolasi, V.; Pretto, L.; Gilli, G. *J. Mol. Struct.* **2006**, *790*, 40–49.
(54) CSD codes: BEKHAB, BIHNUC, CABWAE, CICCUN, DEHMIN, DEHMOT, DEHMUZ, DEHNAG, DEHNEK, DEHNIO, DEHNOU, DEHNUA, DEHPAI, DOTQIN, DUNION, HIQZOX, JARPEX, JATJIX, JAYREH, KAQSAW, KIBJOU, LEMQID, LEZHIH, LEZHON, MAMMEU, MAMMIY, NQNCPH, OGUWES, OGUXAP, OLOCAT, PAHGUB, PAMBOO, POYSUS, POYTAZ, POYTED, SCNPHO, SIWVUP, SOQQIY, VEHXIP, VEHXOV, WIKWOC, WIKWUI, WIKXAP, WIKXET, ZUCQET, ZUCQIX, ZUCQOD, ZUCQUJ, ZUCRAQ.
(55) Kelemen, J.; Kormány, G.; Rihs, G. *Dyes Pigm.* **1982**, *3*, 249–271.
(56) Grainger, C. T.; McConnell, J. F. *Acta Crystallogr.* **1969**, *B25*, 1962–1970.
(57) Guggenberger, L. J.; Teufer, G. *Acta Crystallogr.* **1975**, *B31*, 785–790.
(58) Schmidt, M. V.; Buchsbaum, C.; Schnorr, J. M.; Hofman, D. W. M.; Ermrich, M. *Z. Kristallogr.* **2007**, *222*, 30–33.
(59) Yatsenko, A. V.; Paseshnichenko, K. A.; Chernyshev, V. V.; Schenk, H. *Acta Crystallogr.* **2001**, *E57*, o1151–o1153.
(60) Pendergrass, D. B.; Paul, I. C.; Curtin, D. Y. *J. Am. Chem. Soc.* **1972**, *94*, 8730–8737.
(61) Schmidt, M. U.; Brüning, J.; Wirth, D.; Botle, M. *Acta Crystallogr.* **2008**, *C64*, o474–o477.
(62) Berrie, A. H.; Hampson, P.; Longworth, S. W.; Mathias, A. *J. Chem. Soc. B* **1968**, 1308–1310.
(63) Kelemen, J.; Moss, S.; Glitsch, S. *Dyes Pigm.* **1984**, *5*, 83–108.
(64) Yu, Y.; Qian, K. *Acta Crystallogr.* **2009**, *E65*, o2033.
(65) Turro, N. J. *Modern Molecular Photochemistry*; University Science Books: Sausalito, CA, 1991.

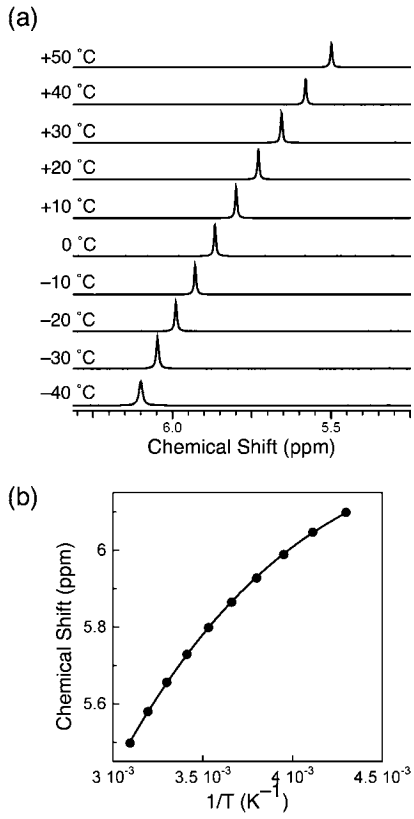

Figure 8. (a) Partial ^{1}H NMR spectra (400 MHz) of **7** in $CDCl_3$ (10 mM) showing the O−H proton resonance as a function of temperature from −40 to +50 °C. (b) Plot of δ_{obs}(O−H) vs $1/T$ (●) overlaid with the fit (gray line). See the text for the values of the thermodynamic parameters ΔH and ΔS derived from nonlinear curve fitting and Scheme 7 for the model used.

Å; Figure S4 in the Supporting Information) to a neighboring molecule in the lattice. Such a structural deviation from ideal threefold symmetry arises from solid-state packing interactions that promote intermolecular contacts, which are unlikely to occur in solution phase. In support of this notion, the ^{1}H NMR spectrum of **7** in $CDCl_3$ at $T = 298$ K shows a single sharp O−H proton resonance of the tertiary alcohols at 5.72 ppm (Figure 8a) that is significantly downfield-shifted relative to that of **6** (2.16 ppm) (Scheme 3). Within the 2−36 mM concentration range, the O−H proton resonances of **7** remain essentially invariant, which is consistent with their involvement in an intramolecular hydrogen bonding network, as supported by the DFT-optimized geometry of the structure (Figure 3).

As shown in Figure 8a, variable-temperature (VT) ^{1}H NMR studies on **7** from +50 to −40 °C revealed a systematic downfield shift of the O−H proton resonance from 5.49 to 6.09 ppm with decreasing temperature. This behavior can best be explained by a fast exchange between the folded (**7F**) and unfolded (**7U**) conformers, which gives rise to a population-averaged δ_{obs} value (Scheme 7).[22] This experimental observable could be fitted using an idealized two-state model[66] with contributions of δ_{7F} (from **7F**) and δ_{7U} (from **7U**), which exist in mole fractions of x and $1 - x$, respectively, in solution. In this model, the increasing population of the folded conformation **7F** through reinforced hydrogen bonding at lower temperatures

(66) The cooperative nature of structural folding (see ref 21) would cause the system to approximate the "all-or-nothing" situation as depicted in Scheme 7, but partially folded/unfolded conformations deviating from the ideal threefold symmetry might also contribute to δ_{obs}.

Scheme 7. Temperature-Dependent Structural Folding and Unfolding

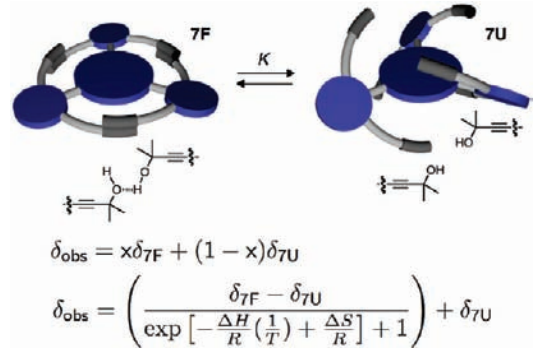

is reflected in the deshielding of the O−H protons and systematic downfield shifts.

The temperature-dependent chemical shift of **7** was subsequently analyzed using a δ_{obs} versus $1/T$ plot (Figure 8b) on the basis of the model shown in Scheme 7. With the δ_{7U} value of 2.02 ppm obtained from initial fitting, which is close to the non-hydrogen-bonded O−H proton resonance of the free aniline **6** at 2.16 ppm, further nonlinear regression was carried out to provide the values $\delta_{7F} = 6.31 \pm 0.01$ ppm, $\Delta H = 2.43 \pm 0.04$ kcal mol^{-1}, and $\Delta S = 4.6 \pm 0.1$ cal mol^{-1} K^{-1}. These parameters are comparable to those obtained for a tris(*N*-salicylideneamine)-based system ($\Delta H = 2.2 \pm 0.1$ kcal mol^{-1}; $\Delta S = 4.2 \pm 0.1$ cal mol^{-1} K^{-1})[22] and confirmed the endothermic nature of structural unfolding (positive ΔH). We note that the hydrogen bonding in the tris(hydrazone) molecular core of **7** is unaffected under these condition (Figures S2 and S3 in the Supporting Information).

Photophysical Consequences of Bond Twisting. In $CHCl_3$ at $T = 25$ °C, compounds **7**−**9** display intense electronic transitions as two broad peaks that are separated by $\Delta\lambda = 100-127$ nm (Figure 9). In the case of **4**, such features were previously assigned as individual contributions from the azo (for the shorter-wavelength transition) and hydrazone (for the longer-wavelength transition) tautomers, respectively.[24] Our solution NMR studies, DFT calculations, and single-crystal X-ray analysis described in previous sections, however, strongly suggest that both absorption bands arise from the hydrazone tautomer, which dominates the solution population.

Intriguingly, the 2,6-substituents on the peripheral aryl rings profoundly impact the photophysical properties of the homologous series of tris(hydrazone) chromophores **7**−**9**. As shown in Figure 9, a systematic blue shift in electronic absorption was observed along the series **7** → **8** → **9**. This trend nicely correlates with an increase in the torsional angle (τ) between the planar conjugated tris(hydrazone) core and the peripheral aryl groups. As shown in Figures 3 and 4, the O−H···O−H hydrogen bonding between the ethynylene-extended 2,6-substituents on the aniline rings promotes structural collapse with the relatively small dihedral angles of $\tau = 24°$ in the DFT model $\mathbf{7'_H}$ and $\tau = 19-25°$ in structurally characterized **7**. On the other hand, steric constraints imposed by the bulky 2,6-diisopropyl substituents in **9** enforce large dihedral angles of $\tau = 54-65°$ (Figure 3). Such a conformation effectively minimizes undesired van der Waals contacts, as previously observed in the X-ray structure of a similar tris(*N*-salicylideneamine) derivative.[17] Sterically "neutral" compound **8**, having neither attractive (as in **7**) nor

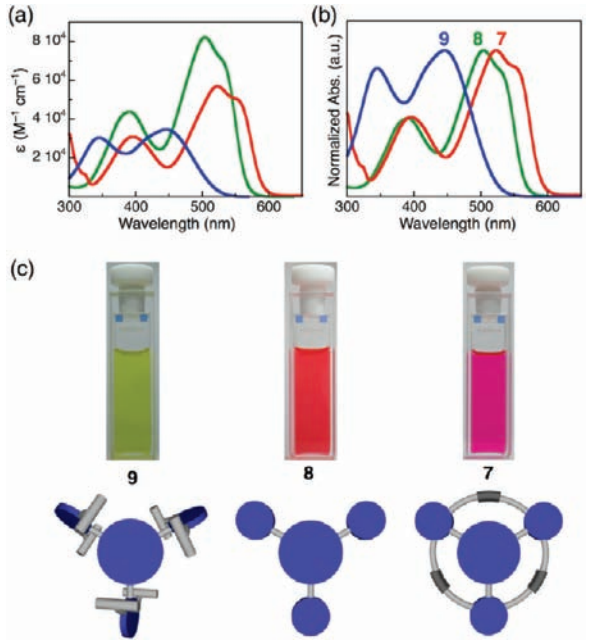

Figure 9. (a) UV−vis spectra of **7** (red), **8** (green), and **9** (blue) in $CHCl_3$ at 25 °C. (b) Normalized UV−vis spectra of **7** (red), **8** (green), and **9** (blue) for comparison of structure-dependent spectral shifts. (c) Photographic images of $CHCl_3$ solutions of **7**−**9** (concentration = 0.02 mM) and schematic representations of the corresponding molecular structures. Steric crowding enforces deconjugation between the molecular core and the peripheral aryls in **9**, while hydrogen-bonding-assisted planarization promotes long-range electronic conjugation in **7**.

repulsive (as in **9**) steric bias, is thus anticipated to sample a wider window of τ values without significant energetic gain or penalty.

An intuitive particle-in-a-box model would thus suggest that a progressive shrinkage in the electronic conjugation along the series **7** → **8** → **9** would translate into increasing energy gaps between the molecular orbitals (MOs) involved in the electronic transition and therefore shift the UV−vis absorption to shorter wavelengths (Figure 9).[15] Because of a large shift in the longer-wavelength transitions (**7**, λ_{max} = 523 nm; **8**, λ_{max} = 505 nm; **9**, λ_{max} = 445 nm), the color difference could be detected even by the naked eye (Figure 9c).

Solvent-Driven Conformational Switching. The active role played by the intramolecular hydrogen bonds in the structural interconversion (Scheme 7) prompted the investigation of molecule−solvent interactions in conformational switching. An additional point of consideration within this context was whether the tautomeric equilibrium of the tris(hydrazone) molecular core would also shift in response to external stimuli.[43,48,67−69]

As shown in Figure 10c, the normalized UV−vis spectra of **8** in DMSO and $CHCl_3$ are essentially superimposable, indicating that the electronic structure of the tris(hydrazone) core remains largely unperturbed upon changes in solvent polarity or hydrogen-bonding ability. This observation is also consistent with the ^1H and ^{13}C NMR data (Figures 1 and 2), which confirmed the solvent-invariant nature of the tris(hydrazone) tautomer.

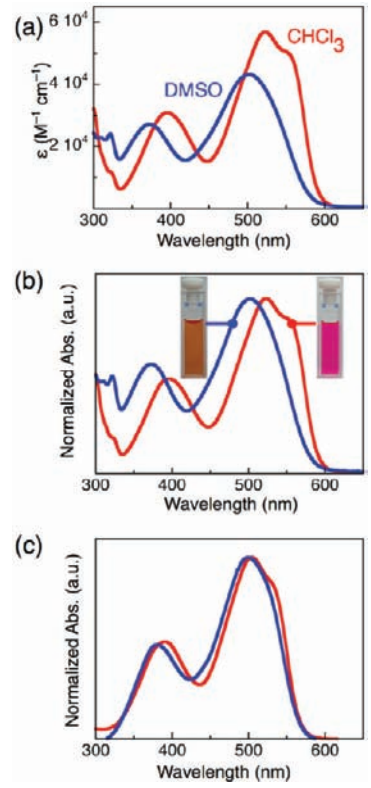

Figure 10. (a) UV−vis spectra of **7** in $CHCl_3$ (red) and DMSO (blue). (b) Normalized UV−vis spectra of **7** in $CHCl_3$ (red) and DMSO (blue); the insets show photographic images of the corresponding solutions (concentration = 0.02 mM). (c) Normalized UV−vis spectra of **8** in $CHCl_3$ (red) and DMSO (blue).

Table 4. UV−Vis Data for **7** and **8** in Selected Solvents (T = 298 K)

compound	solvent	λ_{max} (nm)
7	hexane	517, 391
	toluene	523, 395
	$CHCl_3$	523, 396
	THF	516, 386
	acetone	506, 384
	MeCN	496, 385
	MeOH	506, 379
	DMSO	502, 373
8	$CHCl_3$	505, 392
	MeOH	498, 386
	DMSO	499, 382

In contrast, the UV−vis spectra of **7** in hydrogen-bonding solvents such as DMSO and MeOH show significant ($\Delta\lambda \approx 20$ nm) blue shifts relative to those taken in non-hydrogen-bonding solvents such as toluene and $CHCl_3$ (Figure 10a,b; see Table 4 for a summary of the UV−vis spectral data of **7** and **8** in representative solvents). This observation can be rationalized by the O−H···(solvent)$_n$ interactions in **7** that would compete with the intramolecular O−H···O−H hydrogen bonds to trigger structural unfolding (Scheme 8).

An increase in the torsional angles between the molecular core and the peripheral aryl groups in this unfolded conformer,

(67) Reeves, R. L.; Kaiser, R. S. *J. Org. Chem.* **1970**, *35*, 3670–3675.
(68) Kelemen, J. *Dyes Pigm.* **1981**, *2*, 73–91.
(69) For tautomer switches based on azo functional groups, see: (a) Antonov, L.; Deneva, V.; Simeonov, S.; Kurteva, V.; Nedeltcheva, D.; Wirz, J. *Angew. Chem., Int. Ed.* **2009**, *48*, 7875–7878. (b) Farrera, J.-A.; Canal, I.; Hidalgo-Fernandez, P.; Perez-Garcia, M. L.; Huertas, O.; Luque, F. J. *Chem.—Eur. J.* **2008**, *14*, 2277–2285. (c) Matazo, D. R. C.; Ando, R. A.; Borin, A. C.; Santos, P. S. *J. Phys. Chem. A* **2008**, *112*, 4437–4443. (d) Nihei, M.; Kurihara, M.; Mizutani, J.; Nishihara, H. *J. Am. Chem. Soc.* **2003**, *125*, 2964–2973. (e) Kao, T.-L.; Wang, C.-C.; Pan, Y.-T.; Shiao, Y.-J.; Yen, J.-Y.; Shu, C.-M.; Lee, G.-H.; Peng, S.-M.; Chung, W.-S. *J. Org. Chem.* **2005**, *70*, 2912–2920.

Scheme 8. Structural Folding and Unfolding Induced by Solvent−Molecule Interactions

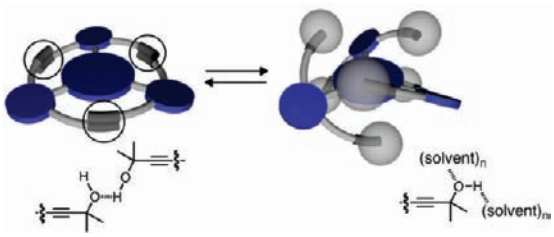

in a manner similar to the situation in **9** (Figure 9), would suppress the long-range electronic conjugation and elicit spectral blue shifts. A conceptually related process was observed for tris(*N*-salicylideneamine)-based molecular switches that respond to polar solvents by changing the emission quantum yield[18,20] or reversing the screw sense of the helical structure.[22] The validity of this working hypothesis was subsequently tested using volatile amines as potential hydrogen-bonding agents toward **7**.

Colorimetric Detection of Hydrogen-Bonding Amines. The solvent-dependent color change induced by structural folding and unfolding of **7** (Figure 10 and Scheme 8) stimulated the investigation of its response toward volatile amines that function as potential hydrogen-bonding donors and/or acceptors. Thin films of **7** ($\lambda_{max} = 519$ nm) and **8** ($\lambda_{max} = 503$ nm) were prepared by drop-casting $CHCl_3$ solution samples (1.0 mM) onto glass substrates. As shown in Figure 11, the electronic absorption spectra of these solid-state samples are essentially identical to those measured for $CHCl_3$ solution samples (Figure 10), indicating that (i) the tautomeric and conformational structures of the molecule are maintained even after aggregation and (ii) no significant interchromophore electronic coupling exists in the condensed phase.

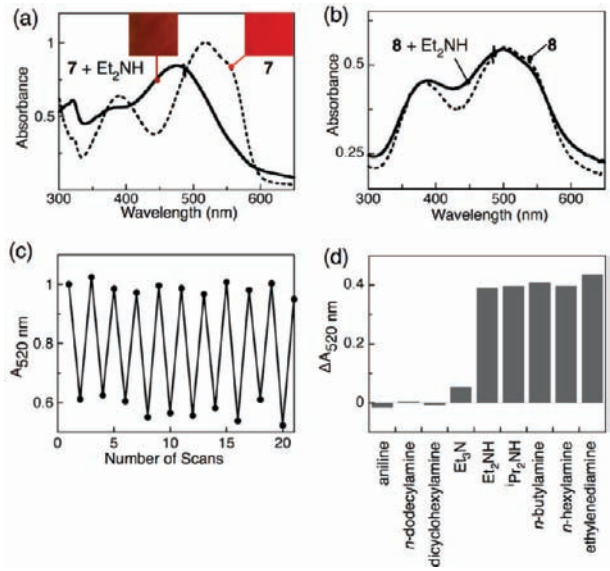

Figure 11. UV−vis spectra of thin films of (a) **7** and (b) **8** before (dotted line) and after (solid line) exposure to a saturated vapor of diethylamine under ambient conditions. In (a), photographic images are also shown in the inset. (c) Color switching of the thin film of **7** monitored by the absorbance change at 520 nm upon repeated cycles of adsorption of diethyamine vapor and desorption by heating (5 s at 100 °C). (d) Response profile of the thin film of **7** toward saturated amine vapors under ambient conditions monitored by ΔA_{520nm}. Thin-film samples were prepared by drop-casting of 1.0 mM solution samples of **7** and **8** onto glass substrates.

A brief exposure of the thin-film sample of **7** to diethylamine vapor in the air, however, resulted in a dramatic color change from pink to dark-orange, with a large hypsochromic shift of the longer-wavelength transition from $\lambda_{max} = 519$ nm to $\lambda_{max} = 478$ nm (Figure 11a). Notably, this spectral change could be reversed by evaporation of the amine after a brief application of heat, and such switching cycles could be repeated >10 times without noticeable deterioration of the performance of the material (Figure 11c). Under similar conditions, however, the thin-film sample of **8** underwent only a slight change in absorption intensity with no shift of the absorption bands (Figure 11b), indicating that a direct interaction between the chromogenic tris(hydrazone) core and the amine substrate is not the origin of the large spectral shifts observed for **7**.

Since Et_2NH can function as either a hydrogen-bond donor or acceptor, its interaction with the peripheral OH groups of **7** is likely to twist the peripheral aryl groups away from effective conjugation with the tris(hydrazone) core in a manner similar to the conformational switching and spectral blue shifts observed in hydrogen-bonding solvents (Figure 10 and Scheme 8). We note that the longer-wavelength spectral shift observed for solid **7** ($\Delta\lambda_{max} = 41$ nm; Figure 11a) is significantly larger than that induced by hydrogen-bonding solvents such as MeOH or DMSO ($\Delta\lambda_{max} = 17-21$ nm; Figure 10 and Table 4). This phenomenon presumably reflects restricted motions of the putative amine complexes of **7** in the solid state. As depicted in Scheme 8, hydrogen-bonding solvent molecules would dynamically interact with the terminal O−H groups to disrupt the structure-rigidifying hydrogen-bonding network. As such, the UV−vis spectrum of **7** shown in Figure 10 reflects an ensemble of folded and unfolded conformers that rapidly exchange in solution. In the case of thin-film samples with slow exchange kinetics, however, a significant portion of **7** is anticipated to retain the twisted (i.e., unfolded) conformation until the adsorbed amines are thermally removed. Presumably, an effective conformational lock in the solid state is responsible for larger spectral shifts through binding-induced structural distortion.

In support of this mechanistic model, our colorimetric detection scheme is generally applicable to a range of primary and secondary amines with relatively low molecular weights (Figure 11d). Intriguingly, triethylamine elicited little color change despite the fact that it has a much higher vapor pressure (57.07 mmHg at 25 °C) than *n*-hexylamine (8.99 mmHg at 25 °C) and a similar basicity ($pK_a = 10.56$ for Et_3N; 10.75 for n-$C_6H_{11}NH_2$).[70] This observation indicates that hydrogen-bonding donor ability rather than intrinsic basicity is responsible for the experimentally observed colorimetric response.

Selective recognition of primary, secondary, and tertiary amines *in solution* has previously been demonstrated using sensor arrays consisting of chemoresponsive dyes[71,72] or elaborate multitopic receptor molecules that exploit N−H···O hydrogen bonds and hydrophobic effects.[73] Detection of *vapor samples* of amines having different substitution patterns, however, still remains a significant challenge. Practical ap-

(70) *CRC Handbook of Chemistry and Physics*, 90th ed. (Internet version 2010); Lide, D. R., Ed.; CRC Press/Taylor and Francis: Boca Raton, FL, 2010.
(71) Zhang, C.; Suslick, K. S. *J. Am. Chem. Soc.* **2005**, *127*, 11548–11549.
(72) Montes-Navajas, P.; Baumes, L. A.; Corma, A.; Garcia, H. *Tetrahedron Lett.* **2009**, *50*, 2301–2304.
(73) (a) Jung, J. H.; Lee, S. J.; Kim, J. S.; Lee, W. S.; Sakata, Y.; Kaneda, T. *Org. Lett.* **2006**, *8*, 3009–3012. (b) Jung, J. H.; Lee, H. Y.; Jung, S. H.; Lee, S. J.; Sakata, Y.; Kaneda, T. *Tetrahedron* **2008**, *64*, 6705–6710.

proaches often employ perturbations of delocalized electronic structures associated with $\pi-\pi$-stacked organic molecules[74] or conjugated polymers,[75] which give rise to changes in their optoelectronic properties. Statistical analysis on colorimetric sensor arrays has also complemented such efforts.[76] The torsion-induced changes in electronic properties described in the current work offer an alternative signal transduction mechanism that exploits predictable and controllable molecular motions.

Summary and Outlook

New C_3-symmetric conjugated molecules based on a tris(hydrazone) platform were prepared by simple triple azo coupling reactions. A combination of solution $^1H/^{13}C$ NMR and UV−vis spectroscopy, single-crystal X-ray crystallography, and DFT computational studies provided compelling evidence for the existence of a keto−hydrazone rather than an enol−azo tautomeric core, which gives rise to characteristic longer-wavelength UV−vis absorption bands at $\lambda_{max} = 445-523$ nm. The branched $[n,\pi]$ conjugation responsible for these intense visible transitions can be modulated through twisting of the C−N bonds that connect the molecular core to the peripheral aryl groups. Notably, this molecular switch could be driven by the assembly and disassembly of a hydrogen-bonding network through interaction with exogenous agents. A signal transduction mechanism that exploits such binding-induced conformational transitions was implemented for thin-film samples that undergo reversible color switching upon exposure to selected primary and secondary amine vapors. Efforts to expand the scope of this chemistry by structurally engineering these proof-of-principle prototypes to target an expanded set of analytes are underway.

Experimental Section

General Considerations. All of the reagents were obtained from commercial suppliers and used as received, unless otherwise noted. The compound 4-*tert*-butyl-2,6-diiodoaniline was prepared according to a literature procedure.[77] All air-sensitive manipulations were carried out under a nitrogen atmosphere using standard Schlenk line techniques.

Physical Measurements. ^1H and ^{13}C NMR spectra were recorded on a 300 MHz Varian Gemini 2000 or 400 MHz Varian Inova NMR spectrometer. Chemical shifts were reported versus tetramethylsilane and referenced to the residual solvent peaks. High-resolution electrospray ionization mass spectrometry (HR ESI-MS) was performed on a Thermo Electron Corporation MAT 95 XP-Trap mass spectrometer. FT-IR spectra were recorded on a Nicolet Avatar 360 FT-IR spectrometer with EZ OMNIC ESP software. UV−vis spectra were recorded on a Varian Cary 5000 UV−vis−NIR spectrophotometer.

2,6-Bis(3-methyl-3-hydroxyl-1-butynyl)-4-*tert*-butylaniline (6). A round-bottom flask was charged with 4-*tert*-butyl-2,6-diiodoaniline (1.83 g, 4.56 mmol), 2-methylbut-3-yn-2-ol (860 mg, 10.2 mmol), $^iPr_2NH$ (20 mL), $PdCl_2(PPh_3)_2$ (81.2 mg, 0.115 mmol), CuI (43.1 mg, 0.225 mmol), and THF (40 mL). The mixture was purged with N_2, stirred for 24 h at room temperature (rt), and concentrated under reduced pressure. Flash column chromatography on SiO_2 [hexanes/EtOAc = 2:1 to 1:1 (v/v)] furnished **6** as a yellow solid (1.32 g, 4.21 mmol, 92%). ^1H NMR (400 MHz, $CDCl_3$, 298 K): δ 7.24 (s, 2H), 4.53 (s, 2H), 2.16 (s, 2H), 1.62 (s, 12H), 1.22 (s, 9H). ^{13}C NMR (100 MHz, $CDCl_3$, 298 K): δ 146.2, 140.3, 129.7, 106.8, 99.3, 78.9, 65.9, 33.9, 31.8, 31.4. FT-IR (thin film on NaCl, cm^{-1}): 3374, 2967, 2867, 2216, 1609, 1583, 1461, 1411, 1394, 1362, 1327, 1306, 1232, 1192, 1163, 972, 941, 909, 883, 854, 734, 641. HR ESI-MS: calcd for $C_{20}H_{27}NO_2Na$ $[M + Na]^+$, 336.1939; found, 336.1926.

(2*E*,4*E*,6*E*)-2,4,6-Tris(2-(4-*tert*-butyl-2,6-bis(3-hydroxy-3-methylbut-1-yn-1-yl)phenyl)hydrazono)cyclohexane-1,3,5-trione (7). A 20 mL vial was charged with **6** (0.258 g, 0.823 mmol), MeOH (5 mL), 2 M aqueous HCl (3 mL), and a magnetic stir bar. The reaction mixture was cooled to 0 °C using an ice bath and stirred. A precooled (0 °C) aqueous solution (3 mL) of $NaNO_2$ (81.1 mg, 1.17 mmol) was added using a pipet over a period of 10 min, and the reaction mixture was stirred for additional 10 min at 0 °C. A 250 mL round-bottom flask was charged with phloroglucinol dihydrate (31.3 mg, 0.193 mmol), MeOH (20 mL), 2 M aqueous NaOH (3.10 mL), and a magnetic stir bar and cooled to 0 °C. A pipet was used to add the diazonium reaction mixture containing **6** over a period of 20 min. The resulting mixture was stirred for additional 0.5 h at 0 °C and then neutralized by addition of 2 M aqueous HCl. The mixture was diluted with water (100 mL), and the organic fraction was extracted into EtOAc (100 mL × 2) and washed with water (100 mL). Volatile fractions were removed under reduced pressure, and the residual material was purified by flash column chromatography on SiO_2 [hexanes/EtOAc = 4:1 (v/v)] to furnish **7** as a dark-red solid (0.171 g, 0.155 mmol, 81%). A single crystal of **7** suitable for X-ray crystallography was obtained by slow cooling of a boiling saturated CH_3CN solution of this material. ^1H NMR (400 MHz, $CDCl_3$, 298 K): δ 16.4 (s, 3H), 7.48 (s, 6H), 5.72 (s, 3H), 1.59 (s, 36H), 1.33 (s, 27H). ^{13}C NMR (100 MHz, $CDCl_3$, 298 K): δ 178.2, 150.4, 139.5, 131.5, 129.2, 114.7, 101.7, 77.8, 65.2, 34.8, 31.3, 31.1. FT-IR (thin film on NaCl, cm^{-1}): 3423, 1968, 2931, 2869, 1600, 1585, 1474, 1440, 1411, 1394, 1364, 1308, 1239, 1218, 1186, 1071, 1036, 1020, 953, 885, 862. HR ESI-MS: calcd for $C_{66}H_{78}N_6O_9Na$ $[M + Na]^+$, 1121.5728; found, 1121.5747.

(2*E*,4*E*,6*E*)-2,4,6-Tris(2-(4-*tert*-butylphenyl)hydrazono)cyclohexane-1,3,5-trione (8). This compound was prepared using 4-*tert*-butylaniline (0.505 g, 3.38 mmol) and phloroglucinol dihydrate (0.117 g, 0.721 mmol) in a manner similar to that described for **7**. The product was isolated as a bright-red solid (0.151 g, 0.247 mmol, 34%) after flash chromatography on SiO_2 [hexanes/EtOAc = 10:1 to 4:1 (v/v)]. ^1H NMR (400 MHz, $CDCl_3$, 298 K): δ 16.4 (s, 3H), 7.59 (d, J = 11.6 Hz, 6H), 7.48 (d, J = 11.2 Hz, 6H), 1.35 (s, 27H). ^{13}C NMR (100 MHz, $CDCl_3$, 298 K): δ 178.7, 151.2, 139.0, 128.7, 126.8, 117.5, 34.9, 31.4. FT-IR (thin film on NaCl, cm^{-1}): 2963, 2926, 2869, 1601, 1471, 1436, 1409, 1364, 1308, 1241, 1172, 1098, 1054, 843. HR ESI-MS: calcd for $C_{36}H_{43}N_6O_3$ $[M + H]^+$, 607.3397; found, 607.3372.

(2*E*,4*E*,6*E*)-2,4,6-Tris(2-(2,6-diisopropylphenyl)hydrazono)cyclohexane-1,3,5-trione (9). This compound was prepared using 2,6-diisopropylaniline (0.304 g, 1.71 mmol) and phloroglucinol dihydrate (57.1 mg, 0.352 mmol) in a manner similar to that described for **7**. The product was isolated as a bright-red solid (0.201 g, 0.290 mmol, 82%) after flash chromatography on SiO_2 [hexanes/dichloromethane = 1:1 to 1:2 (v/v)]. ^1H NMR (400 MHz, $CDCl_3$, 298 K): δ 16.0 (s, 3H), 7.27 (t, J = 6.8 Hz, 3H), 7.22 (d, J = 12.8 Hz, 6H), 3.24 (septet, J = 6.8 Hz, 6H), 1.25 (d, J = 6.8 Hz, 36H). ^{13}C NMR (100 MHz, $CDCl_3$, 298 K): δ 178.7,143.4, 136.7, 129.2, 128.8, 123.9, 28.4, 23.7. FT-IR (thin film on NaCl, cm^{-1}): 2959, 2903, 2867, 1601, 1578, 1477, 1421, 1405, 1363, 1320, 1287, 1230, 1171, 1118, 1052, 833. HR ESI-MS: calcd for $C_{42}H_{55}N_6O_3$ $[M + H]^+$, 691.4336; found, 691.4318.

X-ray Crystallographic Studies. The data collection was carried out using synchrotron radiation (λ = 0.41328 Å, diamond 111 monochromator) from the 15-ID ChemMatCARS beamline at the Advanced Photon Source, Argonne National Laboratory, with a frame time of 1 s and a detector distance of 6.0 cm. A yellow needle (approximate dimensions 0.10 mm × 0.03 mm × 0.03 mm) was

(74) (a) Che, Y.; Yang, X.; Loser, S.; Zang, L. *Nano Lett.* **2008**, *8*, 2219–2223. (b) Che, Y.; Zang, L. *Chem. Commun.* **2009**, 5106–5108. (c) Che, Y.; Yang, X.; Zhang, Z.; Zuo, J.; Moore, J. S.; Zang, L. *Chem. Commun.* **2010**, *46*, 4127–4129.
(75) Liu, W.; Pink, M.; Lee, D. *J. Am. Chem. Soc.* **2009**, *131*, 8703–8707.
(76) Rakow, N. A.; Sen, A.; Janzen, M. C.; Ponder, J. B.; Suslick, K. S. *Angew. Chem., Int. Ed.* **2005**, *44*, 4528–4532.
(77) Iskra, J.; Stavber, S.; Zupan, M. *Synthesis* **2004**, 1869–1873.

placed onto the tip of a 0.05 mm diameter glass fiber and mounted on a platform diffractometer equipped with an APEX II detector at 120(2) K. Two major sections of frames were collected with a step size of 0.5° in ϕ and a detector position of −5.0° in 2θ. Data to a resolution of 0.70 Å were considered in the reduction. Final cell constants were calculated from the *xyz* centroids of 2509 strong reflections from the actual data collection after integration (SAINT).[78] The intensity data were corrected for absorption (SADABS).[79] The space group $P\bar{1}$ was determined on the basis of intensity statistics and systematic absences. The structure was solved and refined using SHELXTL.[80] A direct-methods solution was calculated and provided most of the atomic positions from the E map. Full-matrix least-squares/difference Fourier cycles were refined with anisotropic displacement parameters. The hydrogen atoms were placed in ideal positions and refined as riding atoms with relative isotropic displacement parameters. The final full-matrix least-squares refinement converged to R1 = 0.1084, wR2 = 0.2192 (F^2, all data). The remaining electron density was minuscule and located near the *tert*-butyl moieties.

DFT Calculations. All of the calculations were performed using DFT. Geometry optimizations were performed using the Jaguar 6.0 suite of ab initio quantum chemistry programs[81] at the B3LYP/6-31G** level of theory.[82,83] Frequencies were calculated at the same level to gain the zero-point energy and entropy. All of the stationary points were confirmed to be minima by checking the harmonic frequencies. The energies of the optimized structures were reevaluated by additional single-point calculations on each optimized geometry using Dunning's correlation-consistent triple-ξ cc-pVTZ(-f) basis set.[84] Solvation energies were calculated using a self-consistent reaction field (SCRF) method based on accurate numerical solutions of the Poisson−Boltzmann equation.[85] Empirical parameters such as dielectric constant (ε = 4.806, $CHCl_3$) and atomic radii (H, 1.140 Å; C, 1.900 Å) were used to construct the solute surface. Thermodynamic properties were calculated following standard protocol:

$$G_{sol} = G_{gas} + G_{solv} \quad (2)$$

$$G_{gas} = H_{gas} - TS_{gas} \quad (3)$$

$$H_{gas} = E_{SCF} + \mathrm{ZPE} \quad (4)$$

where G_{gas} is the free energy in the gas phase, G_{solv} is the free energy of solvation computed using the continuum solvation model, H_{gas} is the enthalpy in the gas phase, T is the temperature (=298.15 K), S_{gas} is the entropy in the gas phase, E_{SCF} is the self-consistent field energy (i.e., the "raw" electronic energy computed from the SCF procedure), and ZPE is the zero-point energy.

The gas-phase ^{13}C NMR shielding constants σ were calculated from the coupled perturbed Hartree−Fock (CPHF)[86] wave function using Jaguar at the B3LYP/6-31G** level. The value of σ_{ref} for the reference molecule tetramethylsilane (TMS) was calculated using the same basis set and the same method. The chemical shift δ, which is typically what is measured in an NMR experiment, was then calculated as

$$\delta = \sigma_{ref} - \sigma \quad (5)$$

Acknowledgment. This work was supported by the National Science Foundation (CHE 0547251 and CHE 0645381) and the U.S. Army Research Office (W911NF-07-1-0533). Use of the Advanced Photon Source was supported by the U.S. Department of Energy under Contract DE-AC02-06CH11357. ChemMatCARS Sector 15 is principally supported by the National Science Foundation and Department of Energy under Grant CHE-0535644. We thank the Sloan Foundation (Alfred P. Sloan Research Fellowship to D.L.) and the Research Corporation (Cottrell Scholarship to M.-H.B.) for partial support of this work. We thank Dr. Nikolay Tsvetkov for helpful comments.

Supporting Information Available: Additional spectroscopic and computational data and crystallographic data (CIF). This material is available free of charge via the Internet at http://pubs.acs.org.

JA105121Z

(78) *SAINT*; Bruker Analytical X-Ray Systems: Madison, WI, 2009.
(79) Blessing, R. H. *Acta Crystallogr.* **1995**, *A51*, 33–38.
(80) Sheldrick, G. M. *Acta Crystallogr.* **2008**, *A64*, 112–122.
(81) *Jaguar*, version 7.0; Schrodinger, LLC: New York, 2007.
(82) Becke, A. D. *J. Phys. Chem.* **1993**, *98*, 5648–5652.
(83) Lee, C. T.; Yang, W. T.; Parr, R. G. *Phys. Rev. B* **1988**, *37*, 785–789.
(84) Dunning, T. H., Jr. *J. Chem. Phys.* **1989**, *90*, 1007–1023.
(85) (a) Marten, B.; Kim, K.; Cortis, C.; Friesner, R. A.; Murphy, R. B.; Ringnalda, M. N.; Sitkoff, D.; Honig, B. *J. Phys. Chem.* **1996**, *100*, 11775–11788. (b) Friesner, R. A.; Murphy, R. B.; Beachy, M. D.; Ringnalda, M. N.; Pollard, W. T.; Dunietz, B. D.; Cao, Y. X. *J. Phys. Chem. A* **1999**, *103*, 1913–1928. (c) Edinger, S. R.; Cortis, C.; Shenkin, P. S.; Friesner, R. A. *J. Phys. Chem. B* **1997**, *101*, 1190–1197.
(86) Cao, Y.; Beachy, M. D.; Braden, D. A.; Morrill, L.; Ringnalda, M. N.; Friesner, R. A. *J. Chem. Phys.* **2005**, *122*, 224116.